HHS Public Access

Author manuscript

Neurobiol Dis. Author manuscript; available in PMC 2019 April 01.

Published in final edited form as:

Neurobiol Dis. 2018 April ; 112: 91–105. doi:10.1016/j.nbd.2018.01.011.

Changes in resting-state functional connectivity after stroke in a mouse brain lacking extracellular matrix components

Miriana Jlenia Quattromani[#,1,*], **Jakob Hakon**[#,1], **Uwe Rauch**[2], **Adam Q. Bauer**[§,3], and **Tadeusz Wieloch**[§,1]

[1]Laboratory for Experimental Brain Research, Division of Neurosurgery, Department of Clinical Sciences, Lund University, BMC A13, 22184 Lund, Sweden

[2]Department of Experimental Medical Science, Vascular Wall Biology, BMC B12, 22184 Lund, Sweden

[3]Department of Radiology, Washington University, Saint Louis, MO 63110, USA

Abstract

In the brain, focal ischemia results in a local region of cell death and disruption of both local and remote functional neuronal networks. Tissue reorganization following stroke can be limited by factors such as extracellular matrix (ECM) molecules that prevent neuronal growth and synaptic plasticity. The brain's ECM plays a crucial role in network formation, development, and regeneration of the central nervous system. Further, the ECM is essential for proper white matter tract development and for the formation of structures called perineuronal nets (PNNs). PNNs mainly surround parvalbumin/GABA inhibitory interneurons, of importance for processing sensory information. Previous studies have shown that downregulating PNNs after stroke reduces the neurite-inhibitory environment, reactivates plasticity, and promotes functional recovery. Resting-state functional connectivity (RS-FC) within and across hemispheres has been shown to correlate with behavioral recovery after stroke. However, the relationship between PNNs and RS-FC has not been examined. Here we studied a quadruple knock-out mouse (Q4) that lacks four ECM components: brevican, neurocan, tenascin-C and tenascin-R. We applied functional connectivity optical intrinsic signal (fcOIS) imaging in Q4 mice and wild-type (129S1 mice) before and 14 days after photothrombotic stroke (PT) to understand how the lack of crucial ECM components affects neuronal networks and functional recovery after stroke. Limb-placement ability was evaluated at 2, 7 and 14 days of recovery through the paw-placement test. Q4 mice exhibited significantly impaired homotopic RS-FC compared to wild-type mice, especially in the sensory and parietal regions. Changes in RS-FC were significantly correlated with the number of

[*]Corresponding author: Miriana Jlenia Quattromani, miriana.quattromani@med.lu.se, address: Laboratory for Experimental Brain Research, BMC A13, Sölvegatan 17, 22184 Lund, Sweden.

[#]Equal contribution

[§]Joint senior authorship

CONFLICTS OF INTEREST

None.

interhemispheric callosal crossings in those same regions. PT caused unilateral damage to the sensorimotor cortex and deficits of tactile/proprioceptive placing ability in contralesional fore- and hindlimbs, but the two experimental groups did not present significant differences in infarct size. Two weeks after PT, a general down-scaling of regional RS-FC as well as the number of regional functional connections was visible for all cortical regions and most notable in the somatosensory areas of both Q4 and wild-type mice. Q4 mice exhibited higher intrahemispheric RS-FC in contralesional sensory and motor cortices compared to control mice. We propose that the lack of growth inhibiting ECM components in the Q4 mice potentially worsen behavioral outcome in the early phase after stroke, but subsequently facilitates modulation of contralesional RS-FC which is relevant for recovery of sensory motor function. We conclude that Q4 mice represent a valuable model to study how the elimination of ECM genes compromises neuronal function and plasticity mechanisms after stroke.

Keywords

Stroke; Functional connectivity; Extracellular matrix; Perineuronal nets; Mice

INTRODUCTION

Stroke is a major cause of death and severe disability worldwide and is associated with a limited degree of functional recovery (Benjamin et al., 2017). Rehabilitative training is the current evidence-based strategy to improve outcome in stroke patients, although electromagnetic stimulation of the brain and computer gaming show promising results in clinical studies (Hatem et al., 2016). In experimental models, pharmacological interventions and environmental influences stimulate lost brain function (Pekna et al., 2012; Wieloch and Nikolich, 2006). Following stroke, undamaged neurons can undergo plastic responses and neuroanatomical reorganization to replace damaged structural and functional connections. However, the extent of reorganization remains limited by factors that hamper neuronal growth such as extracellular matrix (ECM) molecules (Overman and Carmichael, 2014).

The ECM is known to regulate important processes in brain development, neuronal growth and network formation. It is associated with the structural stabilization of neuronal processes and synaptic contacts during the maturation of the central nervous system (CNS). Remodeling of the ECM both during development and after CNS injury affects synaptic plasticity, neuronal guidance and their regenerative responses (Kwok et al., 2011). Extracellular matrix molecules are also important for callosal development and guidance cues, especially at the level of the midline (Donahoo and Richards, 2009).

The ECM includes chondroitin sulfate proteoglycans (CSPGs) of the lectican family (aggrecan, brevican, neurocan, versican), as well as tenascins. CSPGs and tenascins are components of a specialized form of ECM called perineuronal nets (PNNs) (Celio et al., 1998) which mainly enwrap the neuronal cell body and proximal dendrites of parvalbumin/GABAergic (PV/GABA) inhibitory neurons (Härtig et al., 1994). Recent studies have implicated CSPGs and PNNs in regulating and restricting structural plasticity. Disruption of PNNs by removal of inhibitory CSPGs, neutralization with antibodies or manipulation of

PNNs components may allow experience-dependent plasticity (Pizzorusso et al., 2002; Soleman et al., 2012). Recent studies from our group showed degradation and reduction in the number of aggrecan$^+$ PNNs after experimental stroke and concomitant training through an enriched environment (EE). These results were accompanied by better outcome in several behavioral tests in rats (Madinier et al., 2014; Quattromani et al., 2017).

Recovery of brain functions lost after stroke are not only as a mere consequence of a local structural damage but also due alteration of the physiological state of neural networks connected to the lesion (Corbetta, 2010). This concept also extends to experimental models; implementing comparable functional neuroimaging tools in both rodents and humans is a promising strategy for providing clinical translation. Functional connectivity optical intrinsic signal (fcOIS) has been recently shown to be an optimal tool to address this need (Bauer et al., 2014; White et al., 2011; Hakon et al., 2017). The aim of this study was to further elucidate possible mechanisms of PNN function/disruption after stroke on the molecular and network level. In order to test if the PNNs disruption was responsible for the better functional recovery seen after EE in our previous study (Madinier et al., 2014), we took advantage of a quadruple knock-out mutant mouse model (Q4) which lacks the ECM components brevican, neurocan, tenascin-C and tenascin-R. Q4 mice and relative controls were subjected to photothrombotic stroke (PT) and their neurological deficits assessed at different times during recovery. FcOIS was performed before and 14 days after PT to understand how the lack of specific ECM components affect functional recovery after stroke.

MATERIALS AND METHODS

Ethical standards and experimental animals

Experimental procedures were approved by the Malmö-Lund animal review board (ethical permit M318265-08 and M50-15) and according to the ARRIVE guidelines.

A colony of the Q4 knock-out mice (Rauch et al., 2005) is kept in the animal house of the Faculty of Medicine at Lund University. Q4 female mice 10–15 weeks of age (20–24 grams) were employed in this study. Age-matched female 129S1/SvImJ mice served as controls and were purchased from the Jackson Laboratory (stock #002448). Naïve mice served as non-operated controls relative to mice subjected to photothrombotic stroke (see below). All animals were housed under a 12h light/dark cycle with *ad libitum* access to food and water.

The experimental design of this study is summarized in Figure 1A. All analyses were performed in a blinded fashion to the investigator who performed the experiments.

Photothrombotic stroke

A focal lesion was induced by PT in the left sensorimotor cortex using Rose Bengal (10 mg/ml saline; Sigma) and cold light (KL 1500 LCD, Schott) as previously described (Quattromani et al., 2014; Watson et al., 1985). Briefly, mice were anesthetized with 2% isoflurane in 100% O_2 in a stereotaxic frame. Mice were placed in the prone position with a self-regulating heating pad controlled by a rectal probe to preserve body temperature at 37°C. Rose Bengal was injected in the tail vein and the skin above the skull was incised. A metal adapter was mounted on the fiber optic bundle in order to produce an approximate

irradiation area of 4 × 2 mm^2. The bundle was then positioned on the exposed skull 1 mm lateral and +2/−2 mm anterior/posterior from bregma and the light was turned on at 2750K for 20 minutes. After illumination, mice were allowed to recover and were returned to their home cages.

Paw-placement test

We have used several behavioral tests during recovery after cortical photothrombotic stroke in rats including the pasta test, catwalk, neuroscore, whisker test and the paw-placement test (Madinier et al. 2014). Results showed that most of the employed tests were sensitive to changes between pre- and post stroke performances, but were unable to highlight differences between housing conditions over time (standard, STD, vs enriched environment, EE) due to spontaneous recovery of function in the control (STD) group within the first weeks of recovery. The paw-placement test, on the other hand, displayed a long-lasting deficit still present at 9 weeks of recovery (Madinier et al. 2014). Similar experiments in C57Bl mice, showed persistent deficits in paw-placement function of both paretic paws, and significant recovery in EE housed mice at 7 and 14 days (Hakon et al., 2017; Quattromani et al., 2014), even as late as up to 3 months after stroke (unpublished data). The paw-placement test reflects the tactile-proprioceptive function of the mouse, and is evident when the stroke lesion is positioned in a distinct somatomotor area (De Ryck et al., 1992; Madinier et al., 2014; Quattromani et al., 2014, Hakon et al., 2017). The test is performed in absence of visual and facial contact cues, to ensure that the tactile-proprioception test component was not compensated for within the sensorimotor task. Hence this test rather than measuring executive motor function, is a test of the initiation and control of movement that involves multiple brain areas specifically higher-order sensorimotor cortices such as posterior parietal and secondary motor cortices (Hakon et al., 2017). For testing, mice were hand-held and kept immobile in a horizontal position. Tactile and proprioceptive input was provided when the paw lost contact with the table surface (passive limb movement) and subsequently lightly contacting the paw with the edge of a table. The (un)successful paw-placements onto the edge of the table were noted. Placing scores for each paw were: 0, no placing; 0.5, incomplete and/or delayed placing; 1, immediate, complete placing. The test was performed at day 2, 7 and 14 of recovery by the same investigator.

Animal preparation for functional neuroimaging

Mice preparation followed the previously published protocol (White et al., 2011). Briefly, anesthesia was initiated with an intra-peritoneal injection of ketamine-xylazine (86.9 mg/kg ketamine and 13.4 mg/kg xylazine; Ketaminol, Intervet and Rompun, Bayer). Mice were placed on a heating pad and anesthetic transition was allowed for 10 minutes. The head was secured in a stereotaxic frame, shaved, and a midline incision was made along the scalp. Approximately 1 cm^2 of the skull was exposed, i.e., most of the cerebral cortex was in the camera's field of view. During imaging, the skull was kept moist with mineral oil. Body temperature was maintained at 37°C using a self-regulating heating pad. All mice were imaged 14 days prior (for baseline) and 14 days after PT. After baseline, mice received a subcutaneous injection of 1 ml saline and the antidote Atipamezole (1 mg/kg; Antisedan, Orion Pharma).

FcOIS imaging system

Sequential illumination was provided at four wavelengths by four light emitting diodes (LEDs; 470 nm, 590 nm, 617 nm, 625 nm; M470L3-C1, M590L3-C1, M617L3-C1 and M625L3-C1, respectively, Thorlabs). LEDs were placed around an EMCCD camera (Ixon 897 Ultra, Andor Technologies) approximately 20 cm above the mouse's head. Crossed linear polarizers were placed in front of the LEDs and camera lens to reject specular reflection from entering the lens. The LEDs and the camera were controlled using a custom-written software (MATLAB). Each of the four LEDs had a full frame rate of 30 Hz which required a camera frame rate of 120 Hz. Up to 45 minutes of resting-state data were collected for each mouse in 5-minute sessions.

Image processing

A "white light" image was collected from each mouse brain and was used to create a manually-constructed brain mask as previously described (Bauer et al., 2014; White et al., 2011). All further analyses were performed only on those pixels labeled as "brain". A quality check of the data from all mice excluded any 5-minute data run in which the mean value of the reflected light intensity level over the brain varied (as a function of time) by more than 1% for any wavelength. This quality control resulted in up to 45 minutes of data subsequently analyzed for each mouse. Spectroscopic inversion converted absorption data to oxygenated and deoxygenated hemoglobin concentration changes. Data were filtered over infraslow frequencies (0.009–0.08 Hz) as in previous fcOIS studies (Bauer et al., 2014; Bergonzi et al., 2015; Bumstead et al., 2017; White et al., 2011). For further analysis, each pixel's time series was down-sampled from 30 Hz to 1 Hz. For baseline imaging, global signal regression (GSR) was used. Time traces of all pixels defined as brain were averaged to create a global brain signal which was regressed from every brain pixel. For day 14 imaging, we implemented a multiple signal regression (MSR) approach. Time traces of all pixels within the infarct and those outside were averaged separately to create two separate regressors which were then regressed from all brain pixels simultaneously (Bauer et al., 2014). Lesion segmentation masks were manually determined for each mouse in Photoshop based on tissue contrast and infarct alignment observed in the NeuN staining (white tissue corresponded to infarcted tissue). Medial and lateral coordinates of the lesion from the midline were noted at different bregma levels and imported in MATLAB.

Resting-state functional connectivity measures

Using the Paxinos atlas as reference (Paxinos and Franklin, 2001), seed locations were chosen at coordinates expected to correspond to the left and right primary motor (M1), secondary motor (M2), somatosensory forelimb (SFL), somatosensory hindlimb (SHL), posterior M2 (M2p), posterior-parietal (PP), retrosplenial (RS) and visual (VIS) cortex as described previously (Bauer et al., 2014; White et al., 2011). Seeds were circular and with a diameter of 0.5 mm (approximately 6 pixels). At each seed location, time traces of hemoglobin fluctuations were correlated against those in every other brain pixel to create a seed-based RS-FC map for that seed. Pearson r correlation coefficients were Fisher z-transformed and averaged to generate group-based RS-FC maps. Interregional seed based matrices were constructed reporting RS-FC between each seed-seed pair for all regions.

Changes in interregional RS-FC between groups were quantified for seed-seed pairs with a positive connection at baseline ($z(r) \geq 0.4$).

To examine homotopic RS-FC, each pixel's time trace in the left hemisphere was correlated to its homologue in the right hemisphere, creating a map of homotopic RS-FC for each mouse. We chose to visualize these maps in the left hemisphere. Values of Fisher *z*-transformed homotopic RS-FC maps were averaged across mice to generate group consensus homotopic RS-FC maps. Regional homotopic RS-FC was quantified within brain regions defined by the Paxinos atlas (Paxinos and Franklin, 2001). The set of correlation coefficients between each pixel's time course and all other time courses in the shared brain mask yields a matrix containing all of the RS-FC information over the cortex. For each pixel (node) the number of functional connections (degree) was determined by thresholding these matrices at $z(r) \geq 0.4$. Summing over pixels in the ipsilateral or contralateral hemisphere relative to a candidate pixel produced weighted maps of intra- and inter-hemispheric node degree for each mouse. Group-level maps were created by averaging across mice, and quantified within brain regions defined by the Paxinos atlas (Paxinos and Franklin, 2001).

Tissue collection

After the final imaging session, mice were transcardially perfused with saline and 4% PFA, pH 7.4. Brains were post-fixed overnight in PFA and transferred to a phosphate-buffered 25% sucrose solution. Brains were sectioned with a microtome in 30-μm-thick slices on the coronal plane. Sections were stored at −20°C in a phosphate-buffered antifreeze solution containing ethyleneglycol and glycerol.

Immunohistochemistry

Free-floating brain slices were blocked in blocking solution (5% normal donkey serum and 0.25% Triton X-100 in PBS) for 1h at RT. Slices were incubated overnight at 4°C with lectin and primary antibodies diluted in blocking solution. On the next day, sections were incubated with secondary antibodies at a dilution of 1:400 in blocking solution for 1.5h at RT. For bright field immunohistochemistry, quenching in 3% H_2O_2 and 10% MeOH for 12 minutes preceded the blocking step. The Vectorstain ABC kit (Vector) and 3,3-diaminobenzidine-tetrahydrochloride (DabSafe, Sweden) were used for visualization. The immunostained slices were examined using a bright-field microscope (Olympus BX60, Sweden) or a confocal laser-scanning microscope (Zeiss LSM 510, Germany). The following antibodies were used: monoclonal mouse anti-CSPGs (Cat-315/MAB1581, 1:1000 for fluorescence and 1:3000 for Dab stainings; Millipore), monoclonal rabbit anti-NeuN (MABN140 1:5000; Millipore). Wisteria floribunda agglutinin (WFA, L1516 1:100; Sigma) was used for the detection of PNNs. All secondary antibodies were purchased from Jackson ImmunoResearch. Biotinylated donkey anti-rabbit, Cy3-conjugated donkey anti-mouse, Alexa Fluor 488-conjugated streptavidin were used to reveal primary antibodies or WFA binding.

Luxol fast blue staining

Free-floating sections were mounted on glass and let dry overnight. Sections were immersed in 95% EtOH for 3 minutes and then incubated at 58°C for 15 hours in a 0.1% Luxol fast

blue (LFB) solution (Solvent Blue 38, Sigma; 95% EtOH; glacial acetic acid). Excess stain was removed by short rinses in 95% EtOH and distillated water. Slices were differentiated in a lithium carbonate solution for 5 minutes, immersed in 70% EtOH for 1 minute and rinsed in water. This differentiation step was repeated 6 times. Slices were dehydrated and mounted to a coverslip with standard procedures. Three sections/each mouse were stained with LFB and subjected to quantification of myelin. The three levels were labelled as follows: level 1, 0.98 mm from bregma; level 2, −1.06 mm from bregma; level 3, −2.06 mm from bregma. For each level, the presence of an interhemispheric crossing of the corpus callosum was evaluated and reported (yes/no). The thickness of the corpus callosum was measured in the middle of the hemisphere contralesional to the lesion, approximately 2 mm from midline (ImageJ, NIH). Images were formatted with Adobe Photoshop.

Infarct volumes

Sections ranging from 2.96 to −3.04 mm from bregma were immunostained for NeuN at 0.5 mm intervals. The non-lesioned area of the infarcted hemisphere and the non-lesioned contralesional hemisphere were outlined using ImageJ, and infarct volumes were calculated by integration as previously described (Swanson et al., 1990).

PNN quantification

One coronal section per brain (bregma level: −0.4 mm) was stained for Cat-315 as described in the immunohistochemistry section. Composite micrographs of the whole ipsilateral and contralateral hemispheres were acquired through a ×4 magnification objective using the CellSens Dimension Software (OlympusBX60, Sweden). An optical grid was used to define distances and draw the boundaries of the somatosensory cortex in both hemispheres according to the Paxinos atlas (Paxinos and Franklin, 2001).

Statistics

Statistical analyses were performed using PRISM 7 software (GraphPad) and MATLAB (Mathworks). Based on experience from previous optical imaging studies, a group size of n=9 was selected for each stroke group and n=4 for the naïve animal groups. With this number of animals, using the “resource equation” (Festing and Altman, 2002), we achieve an E-value of 22 suggesting that adding more animals will not increase chances of getting significant results. We have conducted a sample size calculation (G*power) with alpha=0.05, beta=0.8 based on the intrahemispheric RS-FC values for stroke Q4 and stroke 129S1 mice. This resulted in a minimum sample size of n=6–7 for each stroke group. Data are presented as mean ± SEM unless otherwise stated. Because the SEM takes into account both the SD and the sample size, it indicates the precision of the estimated population mean and is useful for calculating confidence intervals. Values were accepted as significant if $P < 0.05$. A two-tailed unpaired Student’s t-test was used for all comparisons except for behavioral analysis where the Mann-Whitney U-test was employed, and for quantification of the corpus callosum thickness, where one-way ANOVA followed by Bonferroni correction was used. For imaging data, Pearson’s r correlation coefficients were Fisher *z*-transformed prior to all statistical comparisons. Whole-brain, pixel-based difference maps were thresholded at $P < 0.05$, uncorrected. For seed based matrices, differences between groups were analyzed with a two-tailed unpaired Student’s *t*-test followed by FDR correction. Homotopic and node

degree RS-FC measures were analyzed with a two-way ANOVA with groups being one variable and brain area being the repeated measure; two-way ANOVA results were followed by FDR correction.

RESULTS

Infarct size and behavioral performance of Q4 and 129S1 mice after stroke

PT caused unilateral damage to the sensorimotor cortex (Figure 1B). Fourteen days after PT the average infarct volume for the 129S1 group was 10.7 ± 1.69 mm^3 and 11.9 ± 1.41 mm^3 for the Q4 group (Figure 1C). The infarct produced deficits of tactile/proprioceptive placing ability in the contralesional (right) forelimb and/or hindlimb which were visible at day 2, 7 and 14 of recovery. The function of the ipsilesional paws (left) was unaffected by PT. For all testing sessions, the minimum score for both right forelimb and hindlimb was 0 points and the maximum was 2 points. Deficits were still present at 2 days after PT (Figure 1D), when more than half of the Q4 mice showed a complete deficit in the limb-placement ability of both paws (combined score of 0). However, at this time point none of the 129S1 mice showed complete deficits of the paretic limbs (day 2: $P < 0.01$). At day 7 of recovery, all Q4 mice showed a score = 1 signifying partial recovery in the test, but the 129S1 mice performed better (day 7: $P < 0.05$). At 14 days of recovery the differences in scores observed at earlier time points disappeared and both groups showed similar recovery scores.

Resting-state functional connectivity at baseline

Seed based functional connectivity—To investigate the relationship between changes in ECM composition and RS-FC, we used fcOIS imaging to examine RS-FC magnitude in Q4 and 129S1 mice. For every mouse we examined RS-FC patterns for 8 seed locations in each hemisphere. Group-averaged maps were calculated for each seed location at baseline (Figure 2). Positive correlations were shown in red and were mainly present in functionally-related regions, whereas negative correlations were shown in blue and largely between anterior and posterior regions. At baseline, comparable intrahemispheric RS-FC patterns between the two experimental groups were seen for all seeds locations, except for the somatosensory forelimb (SFL) seed that exhibited more prominent patterns of RS-FC in motor regions in the Q4 group compared to 129S1. Non-injured 129S1 and Q4 mice displayed bilaterally-symmetric RS-FC patterns for M1 seeds placed in both left (Figure 2A) and right (Figure 2B) hemispheres. In addition, SFL, somatosensory hindlimb (SHL), posterior parietal (PP), retrosplenial (RS) and visual (VIS) seeds produced symmetric patterns of positive correlation in the 129S1 group (Figure 2A–B, first row). However, these seeds generally exhibited less prominent interhemispheric RS-FC patterns in the Q4 group compared to 129S1 (Figure 2A–B, second row), in particular in the SHL area. Quantitative analysis of regional RS-FC suggested that SFL, SHL and motor cortices exhibit appreciable differences in RS-FC structure across groups; however, no significant differences were observed after FDR correction (Figure 2C–D).

Homotopic functional connectivity—To determine whether changes in ECM composition were associated with reduced bilateral RS-FC, maps of brain wide homotopic RS-FC for the Q4 and 129S1 groups were calculated at baseline (Figure 3). In line with

previous reports (Bauer et al., 2014; Bergonzi et al., 2015; Bero et al., 2012; Bumstead et al., 2017) RS-FC between homotopic regions was largely positive over the cortex in both 129S1 and Q4 mice (Figure 3A). Moderate correlations were seen between homotopic M1, SFL, M2p, RS, and VIS areas in both groups. Q4 mice exhibited significantly lower homotopic RS-FC compared to 129S1 mice in the SHL ($P = 0.007$) and PP ($P = 0.004$) areas (Figure 3A′–A″).

Maps of regional node degree—Node degree maps (Figure 3B–B″) were calculated to examine the number of ipsilateral (intrahemispheric) functional connections for each pixel node at baseline. In both 129S1 and Q4 mice distinct patterns of intrahemispheric node degree were evident for the majority of brain regions (M1, SFL, SHL, PP, and VIS), while moderate node degree was seen in M2p and RS areas (Figure 3B).

Q4 mice had higher intrahemispheric node degree in primary motor areas (Figure 3B′), that was significant in left M1 ($P < 0.05$, Figure 3B″).

Resting-state functional connectivity after stroke

Seed based functional connectivity—To examine RS-FC changes in distinct functional networks after stroke, seed-based RS-FC maps were calculated for both experimental groups. Appreciable disruption in patterns of intra- and inter-hemispheric RS-FC were observed 14 days after stroke in both the 129S1 and Q4 groups (Figure 4).

However, in the ipsilesional hemisphere Q4 mice showed higher RS-FC for seeds placed in left SFL, PP and VIS regions compared to the 129S1 mice (Figure 4A). Similarly, intrahemispheric RS-FC patterns in the contralesional hemisphere of Q4 mice also exhibited higher RS-FC in M1, M2p, SHL and PP cortices compared to 129S1 (Figure 4B). Regional RS-FC for all seeds investigated in the Q4 and 129S1 groups was calculated 14 days after stroke (Figure 4C). In the contralesional hemisphere, intrahemispheric RS-FC between the SHL and M2p areas was significantly higher in Q4 compared to the 129S1 mice (Figure 4D) following FDR correction. Within the contralesional hemisphere, higher interregional RS-FC was observed between SHL and the PP seeds as well as between the M2p and the RS seeds, though these differences did not survive correction for multiple comparisons.

Homotopic functional connectivity maps—RS-FC between interhemispheric homotopic brain regions has been shown to correlate with acute behavioral deficits and long-term recovery after stroke (Bauer et al., 2014; Carter et al., 2010; Silasi and Murphy, 2014). To evaluate how our PT model influences cortical homotopic RS-FC in a mouse model of PNN disruption, group differences (Q4 minus 129S1) in homotopic RS-FC were calculated 14 days after stroke (Figure 5A–5A″). Fourteen days after stroke connections between homotopic regions appeared to be markedly affected by stroke and were abolished (for baseline *vs* day 14 comparisons see Table 1). In particular, a down-scaling of homotopic RS-FC was visible for lesioned and peri-lesioned areas, such as M1, SFL, and SHL (Figure 5A). Moderate correlations were still seen between homotopic M2p, PP, VIS and especially in RS areas, but no statistical differences in homotopic RS-FC strength were observed when comparing the two experimental groups (Figure 5A′–A″).

Maps of regional node degree—We therefore examined the node degree (number of functional connections) that a certain region had with other intrahemispheric brain pixels after stroke. In both experimental groups, stroke reduced the number of intrahemispheric functional connections (node degree RS-FC) in most regions of the left (ipsilesional) hemisphere; for example see M1, SFL, SHL, M2p, PP, and RS cortices (Figure 5B–B″). Except for the M2p and RS areas, all examined regions in the right (contralesional) hemisphere showed a reduction in node degree RS-FC in the 129S1 (Figure 5B), but not the Q4 group. Instead, the Q4 group showed a more "normalized" (baseline) node degree after stroke (for baseline *vs* day 14 comparisons see Table 2). Further, the Q4 group showed significantly increased intrahemispheric node degree RS-FC in contralesional M1 ($P = 0.015$), SHL ($P = 0.002$), and both VIS left ($P < 0.001$) and VIS right ($P < 0.001$) cortices (Figure 5B′–B″).

PNN morphology in animals lacking brevican, neurocan, tenascin-C and tenascin-R

The ECM is known to regulate important processes in brain development, neuronal growth and network formation. Further, recent studies have implicated PNNs in regulating and restricting structural plasticity, which might affect the formation of new functional connections after stroke. In order to investigate the relationship between regional RS-FC and the presence of PNNs, we examined PNNs in Q4 and 129S1 mice subjected to PT through immunostainings of the markers WFA and Cat-315. WFA is a lectin which binds PNNs around PV/GABA interneurons (Härtig et al., 1992). Cat-315 is a marker of aggrecan, the major PNN component, which surrounds neurons in most layers of the cortex with different glycosylation patterns (Matthews et al., 2002). In a recent study we showed that the number and structure of Cat-315$^+$ PNNs in the somatosensory cortex were affected by stroke and concomitant housing in an EE (Madinier et al., 2014). Here we double-stained PNNs for both Cat-315 and WFA markers (Figure 6). In the majority of the cases we observed co-localization of these two markers after PT (Figure 6A″–D″). We rarely observed WFA$^+$ PNNs which were Cat-315$^-$, in both 129S1 and Q4 mice. In 129S1 mice WFA$^+$ PNNs and Cat-315$^+$ PNNs surrounded neuronal cell soma and dendrites (Figure 6A–A″ and 6C–C″). The Q4 mice instead exhibited a remarkable disruption of PNNs compared to 129S1 mice, which was noticeable both in naïve (Supplementary figure 1) and mice subjected to PT. Staining around the dendrites were sometimes absent, and a faint staining was mainly present around the cell soma where a dotted circle around neurons was detectable (Figure 6B-B″ and 6D-D″). Major differences in staining were also present between the ipsilesional (Figure 6A–B) and contralesional hemispheres (Figure 6C–D) in both groups. In general, the ipsilesional hemisphere showed a reduction in the intensity and number of PNNs compared to the contralesional side. Q4 mice revealed a more evident reduction in the appearance of PNNs compared to 129S1 mice (Figure 6B-B″). Quantification of Cat-315$^+$ PNNs at the same bregma distance where we observed RS-FC differences in the somatosensory cortex (Figure 5B′) showed a net reduction in the number of PNNs in Q4 compared to 129S1 mice after PT (Figure 6E; bregma level: −0.4 mm, ***$P < 0.001$).

Corpus callosum hypoplasia in 129S1 and Q4 mice

The corpus callosum is a major white matter tract that facilitates interhemispheric communication in the mammalian brain. To elucidate a potential structural correlate for the

differences in homotopic RS-FC observed after stroke, we examined callosal morphology in mice from both experimental groups. The presence of myelin in the corpus callosum of Q4 and 129S1 mice subjected to experimental stroke was studied with an LFB staining, since LFB binds to the lipoproteins in the myelin sheaths (Figure 7). Changes in callosal integrity were analyzed in the proximity of regions where major variations in homotopic connectivity were observed between the experimental groups after PT (level 1: 0.98 mm; level 2: −1.06 mm; level 3: −2.06 mm from bregma; Figure 7A). In some cases, microscopic analyses of these structures showed an interrupted corpus callosum at the junction of the two hemispheres (see dashed rectangles in Figure 7B). Sections 1 and 3 showed similar results, but section 2 showed major differences between the groups. At this section level, seven 129S1 mice showed midline crossing, but only three Q4 mice showed the same structure (Figure 7C). Comparable results were visible in naïve mice (Supplementary figure 2). The correlation between homotopic RS-FC and the absence/presence of the callosal midline crossing was also analyzed (Supplementary figure 3). At baseline, regional homotopic RS-FC for the SHL, SFL, M2p, PP, RS, and VIS areas correlated with the abscence/presence of the callosal midline crossing. After stroke, homotopic RS-FC was disrupted in the majority of the sensory and motor areas and correlations between corpus callosum integrity and homotopic RS-FC were only maintained for the PP and VIS areas. We next analyzed the thickness of the corpus callosum in the middle of the contralesional hemisphere (dashed line in Figure 7B). Quantification in section 2 showed a significant reduction in corpus callosum thickness in the Q4 group (Figure 7D).

DISCUSSION

Effects of Q4 knock-out on the structure of perineuronal nets

The ECM has attracted increasing attention since the discovery that it plays a key role in the control of CNS plasticity (Pizzorusso et al., 2002), callosal axon guidance and the stabilization of tissue integrity (Donahoo and Richards, 2009). Previous work has generated animals lacking one or more ECM components, such as lecticans and tenascins which form PNNs. Mice deficient for tenascin-C or tenascin-R display impaired LTP (Evers et al., 2002) and diminished plasticity (Bukalo et al., 2001; Cybulska-Klosowicz et al., 2004; Saghatelyan et al., 2001). LTP is also reduced in neurocan (Zhou et al., 2001) and brevican knock-out mice (Brakebusch et al., 2002) where brevican was described to play a key role in gating the function of PV/GABA interneurons, and enabling coordinated circuit responses to experience (Favuzzi et al., 2017). Interestingly, both tenascin mutants develop a phenotype concerning the inhibitory circuitry of the cortex (Irintchev et al., 2005; Nikonenko et al., 2003). The Q4 knock-out mice were described to be able to feed and reproduce normally, without obvious behavioral abnormalities (Geissler et al., 2013; Rauch et al., 2005). In these mice, the dissolution of PNN structures and the upregulation of matrix molecules unusual for the CNS (fibulin-1 and -2) has been described *in vivo* (Rauch et al., 2005). Abnormalities of synaptic structure and function and severe deficits in PNN formation were also described *in vitro* (Geissler et al., 2013).

Here we show that the Q4 mice display very prominent changes in the brain growth-inhibitory ECM structures. In particular, a WFA and Cat-315 double-immunostaining

highlighted the disruption of PNN architecture, which is reminiscent to the structural changes seen in mice subjected to stroke and subsequently housed in an EE (Quattromani et al., 2017). In these studies we showed that rats subjected to stroke and housing in an EE performed better than rats housed in a standard environment (Madinier et al., 2014; Quattromani et al., 2017). We subsequently demonstrated an upregulation of ECM degrading enzymes (MMP-9 and tPA) in animals housed in an EE as well as a reduced number and a degradation of aggrecan^{+} PNNs in the peri-infarct and somatosensory cortex (Quattromaani et al., 2017).

Effects of Q4 knock-out on resting-state functional connectivity

We recently reported that exposure to EE can modulate RS-FC following the same photothrombotic lesion as the present study (Hakon et. al., 2017). Specifically, RS-FC partially recovered in mice housed in an EE for two weeks, particularly in the contralateral hemisphere. Since the morphological changes seen following PT stroke were reminiscent to those seen in naïve Q4 mice, we took advantage of the Q4 knock-out strain to gain further insights into ECM-dependent brain plasticity and its effects on RS-FC.

Prior to stroke, Q4 mice exhibited significant impaired RS-FC between homotopic regions compared to wild-type (129S1 mice). Mice in both 129S1 and Q4 groups were lacking transcallosal crossings, however, Q4 mice displayed a reduced number of interhemispheric crossings and reduced contralesional thickness of the corpus callosum compared to the 129S1 group. Hypoplasia of the corpus callosum has been previously described in the 129 substrain (Balogh et al., 1999). We found that corpus callosum integrity correlated with homotopic RS-FC in most cortical regions for mice in both groups at baseline, but also in regions with preserved homotopic RS-FC after stroke including the PP and VIS areas. Our findings are in line with studies of strain-specific variation in corpus callosum integrity showing robust association between bilateral (homotopic) cortical RS-FC and structural connectivity via the corpus callosum (Schroeter et al., 2016). Because the ECM is essential for proper white matter tract formation, the lack of specific ECM components in the Q4 mice is likely related to disrupted callosal integrity (Meathrel et al., 2002), which could directly impact the temporal coherence of spontaneous brain activity normally exhibited between homotopic brain regions.

After stroke, interhemispheric homotopic RS-FC between most cortical regions declined towards zero in both 129S1 and Q4 mice. However, compared to 129S1 mice, the Q4 mice displayed higher intrahemispheric RS-FC in contralesional sensory and motor cortices after stroke including most of the sensory and motor cortices as revealed by the node degree and seed based RS-FC analyses. The changes in intrahemispheric node degree of the contralateral hemisphere are comparable to those seen in mice recovering from sensorimotor stroke in an EE (Hakon et al, 2017), strongly suggesting a contribution from the contralesional hemisphere in the recovery process. Large volume strokes are associated with greater contralesional cortical plasticity (Carmichael et al., 2017). A recent study in rats treated with anti-NogoA for two weeks after severe unilateral stroke of the sensorimotor cortex presented an initial period (one week) of relatively poor performance in fine forelimb movements, followed by consistently improved performance over time relative to controls

(Lindau et al., 2014). Neuronal NogoA and its receptors are neurite growth inhibitory proteins known to restrict plasticity and stabilize neuronal networks (Delekate et al., 2011). Improvements in behavior after anti-NogoA treatment were related to reorganization of the undamaged (contralateral) motor cortex and increased axonal sprouting from the contralesional corticospinal tract towards denervated areas of the spinal cord (Lindau et al., 2014; Wahl et al., 2014)

Neuroimaging methods using blood-based contrast (e.g. OIS and FMRI) provide an indirect measure of neural activity. Altered hemodynamics within and surrounding lesioned tissue (e.g. due to changes in vascular reactivity or neurovascular coupling) (Lake et al., 2017) could therefore impact measurements of RS-FC. For example, regional temporal delays in spontaneous hemodynamics are one contributor to artifacts in RS-FC measures between intact brain regions and those directly affected by ischemia (Bauer et al., 2014). Temporal lags can be seen in areas of perfusion deficit (Amemiya et al., 2014; Lv et al., 2013; Siegel et al., 2016), as well as in regions exhibiting reduced stimulus-evoked hemodynamic responses (Bauer et al., 2014). Using the hemodynamic activity within the infarct as a nuisance regressor (i.e., via the MSR approach used here) or implementing other lagged RS-FC analyses (Christen et al., 2015; Siegel et al., 2016) can mitigate delay-related effects on RS-FC measures. However, these techniques will not correct for differences in spectral content between regions being correlated (Siegel et al., 2017). It is also important to note that the presence/absence of lag does not necessarily inform the degree of neurovascular uncoupling. For example, in some stroke patients, reduced hemodynamic responses can be present in the absence of lags (Blicher et al., 2012; Rossini et al., 2004; Salinet et al., 2014). Reduced blood flow in lesioned issue, and surrounding changes in collateral flow could also directly affect hemodynamic measures of RS-FC. Because we are measuring correlations (instead of covariance) between cortical regions, small reductions in local hemodynamic responses could have less of an effect on RS-FC compared to delay-based effects. However, the degree to which reduced perfusion affects measures of RS-FC can be profound in cases of severe (>70%) occlusion (Cheng et al., 2012). Despite these potential confounds, OIS and FMRI reveal similar post-stroke changes in RS-FC across multiple species, and corroborate with other modalities that measure neural activity more directly (Mohajerani et al., 2010; Wright et al., 2017). And, because reported relationships between changes in RS-FC and post-stroke behavioral performance are similar between OIS and FMRI, examination of functional network organization after stroke with blood-based imaging methods remains warranted.

Effect of Q4 knock-out on tactile-proprioceptive function

One in two people experience loss in ability to feel everyday objects through touch or know where their limbs are in space after a stroke (Carey, 1995; Kolb et al., 2010; Sullivan and Hedman, 2008). This loss impairs ability to explore the environment and execute everyday tasks such as grasping and manipulating objects. Mice with PT lesions in this study, displayed deficits in the PP test, a test of tactile-proprioceptive function. Although both Q4 and 129S1 groups showed impaired scores in the PP test after stroke, the Q4 mice showed worse impairment compared to the 129S1 group at 2 and 7 days and comparable scores at 14 days of recovery. Because there was no significant difference in the size of the infarct, the

discrepancy in behavioral outcome after stroke could be a result of strain differences in structural or functional connectivity. PNNs provide synaptic stability and protect against excitotoxity and oxidative stress in the early phases after brain injury (Suttkus et al., 2014). Robust structural disruption might have contributed to the worsening of behavioral outcome observed in the Q4 group during the first week of stroke recovery. After 2 weeks of recovery, Q4 mice exhibit behavioral performance comparable to the wild-type group. This “catch-up” in the Q4 group at day 14 might reflect enhanced functional recovery in these mice. Our results in 129S1 mice contrast our previous studies using C57BL mice, with a similar size and location of the infarct, and where mice presented significant deficit in tactile-proprioceptive function at 2 weeks of recovery (Hakon et al., 2017). The incomplete loss of PP function at 2 days after stroke reduces the dynamic range and sensitivity of the test for detecting group-differences in the following weeks of recovery. This is a weakness of the present study, and future experiments are warranted using a more comprehensive test battery to further elucidate the effect of Q4 knock-out on functional recovery after stroke.

Brain plasticity after stroke in Q4 mice

Network remodeling and functional recovery after stroke depend on multiple dynamic biological processes acting concomitant or in series (Wieloch and Nikolich, 2006). Recovery of cell signaling and receptor (AMPA) trafficking are relatively fast processes (hours to days) while dendritic spine modulation and axonal sprouting occurs over longer time periods (days to weeks) (Jones and Schallert, 1992; Lindau et al., 2014; Murphy and Corbett, 2009; Wahl et al., 2014; Wieloch and Nikolich, 2006). Similar to the developing brain, remodeling and reshaping of cortical networks following stroke is experience-dependent and peaks during a critical period (Hensch et. al., 2005). Recent findings in rodents suggest the existence of a similar “critical period” within the first few weeks after stroke when brain plasticity processes are optimally responsive to rehabilitation (Biernaskie et al., 2004; Zeiler et al., 2016). One key aspect of the critical period during development is the transient degradation of PNNs and subsequent formation of new synapses (Hensch, 2005). Degradation of PNNs following stroke is also associated with improved recovery of function (Alia et al., 2016; Madinier et al., 2014; Quattromani et al., 2017) and a sign of plasticity-inducing structural changes occurring over the first two weeks. Even in the presence of disrupted PNNs, the lack of growth-inhibiting ECM components in Q4 mice appears to worsen early behavioral outcome (one week), but could facilitate modulation of contralesional, intrahemispheric RS-FC that supports functional improvement later in the recovery phase (two weeks after stroke).

Many plasticity process are active well beyond the 2 week recovery period studied here, which may not be reflected in cortical RS-FC changes at two weeks (Wieloch and Nikolich, 2006). For example inhibition of myelin-associated, growth-inhibitory factors (or the application of growth-promoting agents) diminish constraints on lesion-induced structural plasticity and induce the formation of new connections one month after stroke (Lindau et al., 2014). Evidently, multiple processes such as PNN modulation and axonal outgrowth are activated at different times after stroke and might contribute to recovery of distinct components of sensorimotor function. Hence further experiments monitoring recovery over

longer time windows than 2 weeks might further elucidate the different recovery profiles of Q4 and 129S1 mice.

CONCLUSIONS

We used a mouse model that lacks four major components of the ECM and observed that the absence of these genes leads to significant changes in RS-FC. Q4 mice exhibited significantly impaired homotopic RS-FC compared to wild-type mice, especially in the sensory and parietal regions. Changes in RS-FC were significantly correlated with the number of interhemispheric callosal crossings in those same regions in both experimental groups. After stroke, Q4 mice exhibited worse behavioral impairment at 2 and 7 days of recovery, but then a comparable score and infarct size when compared to the wild-type group at 14 days of recovery. At this time-point, Q4 mice also exhibited higher intrahemispheric RS-FC in contralesional sensory and motor cortices compared to control mice. We propose that disruption of the dense PNN structures seen in the Q4 mice potentially worsen behavioral outcome in the early phase after stroke but facilitates modulation of contralesional RS-FC in the late recovery phase (two weeks after stroke). We conclude that Q4 mice represent a valuable model to study how the elimination of ECM genes compromises neuronal function and plasticity mechanisms during stroke recovery.

Supplementary Material

Refer to Web version on PubMed Central for supplementary material.

Acknowledgments

The authors wish to acknowledge Carin Sjölund and Kerstin Beirup for excellent technical assistance, and Reinhard Fässler for facilitating the generation of the Q4 mouse strain.

This study was supported by the Swedish Research Council (TW 2011-2652 and 2014-3802), the Hans-Gabriel and Alice Trolle-Wachtmeister Foundation (TW), the Strategic Research Area Multipark (TW), the Pia Ståhl Foundation (TW), the Royal Physiographic Society of Lund (JH, TW and MJQ), the STROKE Riksforbundet (MJQ), and the National Institutes of Health grant 5K25NS08375404 (AQB).

References

Alia C, Spalletti C, Lai S, Panarese A, Micera S, Caleo M. Reducing GABAA-mediated inhibition improves forelimb motor function after focal cortical stroke in mice. Sci Rep. 2016; 6:37823.doi: 10.1038/srep37823 [PubMed: 27897203]

Amemiya S, Kunimatsu A, Saito N, Ohtomo K. Cerebral hemodynamic impairment: assessment with resting-state functional MR imaging. Radiology. 2014; 270:548–55. [PubMed: 24072777]

Balogh S, McDowell C, Stavnezer A, Denenberg V. A behavioral and neuroanatomical assessment of an inbred substrain of 129 mice with behavioral comparisons to C57BL/6J mice. Brain Res. 1999; 31:38–48.

Bauer A, Kraft A, Wright P, Snyder A. Optical imaging of disrupted functional connectivity following ischemic stroke in mice. Neuroimage. 2014; 99:388–401. [PubMed: 24862071]

Benjamin E, Blaha M, Chiuve S, Cushman M, Das S, Deo R, de Ferranti S, Floyd J, Fornage M, Gillespie C, Isasi C, Jiménez M, Jordan L, Judd S, Lackland D, Lichtman J, Lisabeth L, Liu S, Longenecker C, Mackey R, Matsushita K, Mozaffarian D, Mussolino M, Nasir K, Neumar R, Palaniappan L, Pandey D, Thiagarajan R, Reeves M, Ritchey M, Rodriguez C, Roth G, Rosamond W, Sasson C, Towfighi A, Tsao C, Turner M, Virani S, Voeks J, Willey J, Wilkins J, Wu J, Alger H,

Wong S, Muntner P. Heart disease and stroke statistics-2017 update: a report from the American Heart Association. Circulation. 2017; 135:146–603. DOI: 10.1161/CIR.0000000000000485

Bergonzi KM, Bauer AQ, Wright PW, Culver JP. Mapping functional connectivity using cerebral blood flow in the mouse brain. J Cereb Blood Flow Metab. 2014; 35:1–4. DOI: 10.1038/jcbfm.2014.211 [PubMed: 25352045]

Bero AW, Bauer AQ, Stewart FR, White BR, Cirrito JR, Raichle ME, Culver JP, Holtzman DM. Bidirectional relationship between functional connectivity and amyloid-β deposition in mouse brain. J Neurosci. 2012; 32:4334–4340. DOI: 10.1523/jneurosci.5845-11.2012 [PubMed: 22457485]

Biernaskie J, Chernenko G, Corbett D. Efficacy of rehabilitative experience declines with time after focal ischemic brain Injury. 2004; 24:1245–1254. DOI: 10.1523/JNEUROSCI.3834-03.2004

Blicher J, Stagg C, O'Shea J, Østergaard L, MacIntosh B, Johansen-Berg H, Jezzard P, Donahue M. Visualization of altered neurovascular coupling in chronic stroke patients using multimodal functional MRI. J Cereb Blood Flow Metab. 2012; 32:2044–54. [PubMed: 22828998]

Brakebusch C, Seidenbecher CI, Asztely F, Rauch U, Matthies H, Meyer H, Krug M, Bo TM, Zhou X, Kreutz MR, Montag D, Gundelfinger ED, Fa R. Brevican-deficient mice display impaired hippocampal CA1 long-term potentiation but show no obvious deficits in learning and memory. Mol Cell Biol. 2002; 22:7417–7427. DOI: 10.1128/MCB.22.21.7417 [PubMed: 12370289]

Bukalo O, Schachner M, Dityatev A. Modification of extracellular matrix by enzymatic removal of chondroitin sulfate and by lack of tenascin-R differentially affects several forms of synaptic plasticity in the hippocampus. Neuroscience. 2001; 104:359–369. [PubMed: 11377840]

Bumstead JR, Bauer AQ, Wright PW, Culver JP. Cerebral functional connectivity and Mayer waves in mice: phenomena and separability. J Cereb Blood Flow Metab. 2017; 37:471–484. DOI: 10.1177/0271678X16629977 [PubMed: 26868180]

Carey LM. Somatosensory loss after stroke. Crit Rev Phys Rehabil Med. 1995; 7:51–91. DOI: 10.1615/CritRevPhysRehabilMed.v7.i1.40

Carey LM, Oke LE, Matyas TA. Impaired limb position sense after stroke: a quantitative test for clinical use. Arch Phys Med Rehabil. 1996; 77:1271–1278. [PubMed: 8976311]

Carmichael ST, Kathirvelu B, Schweppe CA, Nie EH. Molecular, cellular and functional events in axonal sprouting after stroke. Exp Neurol. 2017; 287:384–394. [PubMed: 26874223]

Carter AR, Astafiev SV, Lang CE, Connor LT, Rengachary J, Strube MJ, Pope DLW, Shulman GL, Corbetta M. Resting interhemispheric functional magnetic resonance imaging connectivity predicts performance after stroke. Ann Neurol. 2010; 67:365–375. DOI: 10.1002/ana.21905 [PubMed: 20373348]

Celio MR, Spreafico R, De Biasi S, Vitellaro-Zuccarello L. Perineuronal nets: past and present. Trends Neurosci. 1998; 21:510–515. DOI: 10.1016/S0166-2236(98)01298-3 [PubMed: 9881847]

Cheng H, Lin C, Soong B, Wang P, Chang F, Wu Y, Chou K, Lin C, Tu P, Lee I. Impairments in cognitive function and brain connectivity in severe asymptomatic carotid stenosis. Stroke. 2012; 43:2567–73. [PubMed: 22935402]

Christen T, Jahanian H, Ni W, Qiu D, Moseley M, Zaharchuk G. Noncontrast mapping of arterial delay and functional connectivity using resting-state functional MRI: a study in Moyamoya patients. J Magn Reson Imaging. 2015; 41:424–30. [PubMed: 24419985]

Corbetta M. Functional connectivity and neurological recovery. Dev Psychobiol. 2010; 54:239–253. DOI: 10.1002/dev.20507 [PubMed: 22415913]

Cybulska-Klosowicz A, Zakrzewska R, Pyza E, Kossut M, Schachner M. Reduced plasticity of cortical whisker representation in adult tenascin-C-deficient mice after vibrissectomy. Eur J Neurosci. 2004; 20:1538–1544. DOI: 10.1111/j.1460-9568.2004.03605.x [PubMed: 15355320]

De Ryck M, Van Reempts J, Duytschaever H, Van Deuren B, Clincke G. Neocortical localization of tactile/proprioceptive limb placing reactions in the rat. Brain Res. 1992; 573:44–60. DOI: 10.1016/0006-8993(92)90112-M [PubMed: 1576535]

Delekate A, Zagrebelsky M, Kramer S, Schwab ME, Korte M. NogoA restricts synaptic plasticity in the adult hippocampus on a fast time scale. Proc Natl Acad Sci U S A. 2011; 108:2569–2574. DOI: 10.1073/pnas.1013322108 [PubMed: 21262805]

Donahoo AS, Richards LJ. Understanding the mechanisms of callosal development through the use of transgenic mouse models. Semin Pediatr Neurol. 2009; 16:127–142. DOI: 10.1016/j.spen.2009.07.003 [PubMed: 19778710]

Evers MR, Salmen B, Bukalo O, Rollenhagen A, Bo MR, Morellini F, Bartsch U, Dityatev A, Schachner M. Impairment of L-type Ca2+ channel-dependent forms of hippocampal synaptic plasticity in mice deficient in the extracellular matrix glycoprotein tenascin-C. J Neurosci. 2002; 22:7177–7194. [PubMed: 12177213]

Favuzzi E, Fernandes C, Ewers H, Rico B, Mantoan L, Maeso P, Fernandes C, Ewers H, Sa A. Activity-dependent gating of parvalbumin interneuron function by the perineuronal net protein brevican. Neuron. 2017; :1–17. DOI: 10.1016/j.neuron.2017.06.028

Festing and Altma. Guidelines for the design and statistical analysis of experiments using laboratory animals. National centre for replacement, refinement, and reduction animals in research. Experimental design/statistics. 2002. Available from http://www.3rs-reduction.co.uk/assets/applets/Festing_Altman.pdf

Geissler M, Gottschling C, Aguado A, Rauch U, Wetzel CH, Hatt H, Faissner A. Primary hippocampal neurons, which lack four crucial extracellular matrix molecules, display abnormalities of synaptic structure and function and severe deficits in perineuronal net formation. J Neurosci. 2013; 33:7742–55. DOI: 10.1523/JNEUROSCI.3275-12.2013 [PubMed: 23637166]

Hakon J, Quattromani MJ, Sjölund C, Tomasevic G, Carey L, Lee JM, Ruscher K, Wieloch T, Bauer AQ. Multisensory stimulation improves functional recovery and resting-state functional connectivity in the mouse brain after stroke. NeuroImage Clin. 2017; 17:717–730. DOI: 10.1016/j.nicl.2017.11.022 [PubMed: 29264113]

Härtig W, Brauer K, Bigl V, Brückner G. Chondroitin sulfate proteoglycan-immunoreactivity of lectin-labeled perineuronal nets around parvalbumin-containing neurons. Brain Res. 1994; 635:307–311. [PubMed: 8173967]

Härtig W, Brauer K, Brückner G. Wisteria floribunda agglutinin-labelled nets surround parvalbumin-containing neurons. Neuroreport. 1992; 3:869–872. [PubMed: 1421090]

Hatem S, Saussez G, Della Faille M, Prist V, Zhang X, Dispa D, Bleyenheuft Y. Rehabilitation of motor function after stroke: a multiple systematic review focused on techniques to stimulate upper extremity recovery. Front Hum Neurosci. 2016; 10:442.doi: 10.3389/fnhum.2016.00442 [PubMed: 27679565]

Hensch TK. Critical period plasticity in local cortical circuits. Nat Rev Neurosci. 2005; 6:877–888. DOI: 10.1038/nrn1787 [PubMed: 16261181]

Irintchev A, Rollenhagen A, Troncoso E, Kiss JZ, Schachner M, Servet M. Structural and functional aberrations in the cerebral cortex of tenascin-C deficient mice. Cereb Cortex. 2005; 15:950–962. DOI: 10.1093/cercor/bhh195 [PubMed: 15537675]

Jones TA, Schallert T. Overgrowth and pruning of dendrites in adult rats recovering from neocortical damage. Brain Res. 1992; 581:156–160. DOI: 10.1016/0006-8993(92)90356-E [PubMed: 1498666]

Kolb B, Teskey GC, Gibb R. Factors influencing cerebral plasticity in the normal and injured brain. Front Hum Neurosci. 2010; 4:204.doi: 10.3389/fnhum.2010.00204 [PubMed: 21120136]

Kwok JCF, Dick G, Wang D, Fawcett JW. Extracellular matrix and perineuronal nets in CNS repair. Dev Neurobiol. 2011; 71:1073–1089. DOI: 10.1002/dneu.20974 [PubMed: 21898855]

Lake E, Bazzigaluppi P, Mester J, Thomason L, Janik R, Brown M, McLaurin J, Carlen P, Corbett D, Stanisz G, Stefanovic B. Neurovascular unit remodelling in the subacute stage of stroke recovery. Neuroimage. 2017:869–882. [PubMed: 27664828]

Lindau NT, Bänninger BJ, Gullo M, Good NA, Bachmann LC, Starkey ML, Schwab ME. Rewiring of the corticospinal tract in the adult rat after unilateral stroke and anti-Nogo-A therapy. Brain A J Neurol. 2014; :739–756. DOI: 10.1093/brain/awt336

Lv Y, Margulies D, Cameron Craddock R, Long X, Winter B, Gierhake D, Endres M, Villringer K, Fiebach J, Villringer A. Identifying the perfusion deficit in acute stroke with resting-state functional magnetic resonance imaging. Ann Neurol. 2013; 73:136–40. [PubMed: 23378326]

Madinier A, Quattromani MJ, Sjölund C, Ruscher K, Wieloch T. Enriched housing enhances recovery of limb placement ability and reduces aggrecan-containing perineuronal nets in the rat

somatosensory cortex after experimental stroke. PLoS One. 2014; 9:e93121.doi: 10.1371/journal.pone.0093121 [PubMed: 24664200]

Matthews RT, Kelly GM, Zerillo CA, Gray G, Tiemeyer M, Hockfield S. Aggrecan glycoforms contribute to the molecular heterogeneity of perineuronal nets. J Neurosci. 2002; 22:7536–7547. [PubMed: 12196577]

Meathrel K, Adamek T, Batt J, Rotin D, Doering LC. Protein tyrosine phosphatase deficient mice show aberrant cytoarchitecture and structural abnormalities in the central nervous system. J Neurosci Res. 2002; 70:24–35. DOI: 10.1002/jnr.10382 [PubMed: 12237861]

Mohajerani M, McVea D, Fingas M, Murphy T. Mirrored bilateral slow-wave cortical activity within local circuits revealed by fast bihemispheric voltage-sensitive dye imaging in anesthetized and awake mice. J Neurosci. 2010; 30:3745–51. [PubMed: 20220008]

Murphy TH, Corbett D. Plasticity during stroke recovery: from synapse to behaviour. Nat Rev Neurosci Neurosci. 2009; 10:861–872. DOI: 10.1038/nrn2735

Nikonenko A, Schmidt S, Skibo G. Tenascin-R–deficient mice show structural alterations of symmetric perisomatic synapses in the CA1 region of the hippocampus. J Comp Neurol. 2003; 349:338–349. DOI: 10.1002/cne.10537

Overman JJ, Carmichael ST. Plasticity in the injured brain: more than molecules matter. Neuroscientist. 2014; 20:15–28. DOI: 10.1177/1073858413491146 [PubMed: 23757300]

Paxinos, G., Franklin, KB. The mouse brain in stereotaxic coordinates. Second. Academic Press; 2001.

Pekna M, Pekny M, Nilsson M. Modulation of neural plasticity as a basis for stroke rehabilitation. Stroke. 2012; 43:2819–2828. DOI: 10.1161/STROKEAHA.112.654228 [PubMed: 22923444]

Pizzorusso T, Medini P, Berardi N, Chierzi S, Fawcett JW, Maffei L. Reactivation of ocular dominance plasticity in the adult visual cortex. Science. 2002; 298:1248–1251. DOI: 10.1126/science.1072699 [PubMed: 12424383]

Quattromani M, Cordeau P, Ruscher K, Kriz J, Wieloch T. Enriched housing downregulates the Toll-like receptor 2 response in the mouse brain after experimental stroke. Neurobiol Dis. 2014; 66:66–73. DOI: 10.1016/j.nbd.2014.02.010 [PubMed: 24613658]

Quattromani MJ, Pruvost M, Guerreiro C, Backlund F, Englund E, Aspberg A, Jaworski T, Hakon J, Ruscher K, Kaczmarek L, Vivien D, Wieloch T. Extracellular matrix modulation is driven by experience-dependent plasticity during stroke recovery. Mol Neurobiol. 2017; doi: 10.1007/s12035-017-0461-2

Rauch U, Zhou XH, Roos G. Extracellular matrix alterations in brains lacking four of its components. Biochem Biophys Res Commun. 2005; 328:608–617. DOI: 10.1016/j.bbrc.2005.01.026 [PubMed: 15694392]

Rossini P, Altamura C, Ferretti A, Vernieri F, Zappasodi F, Caulo M, Pizzella V, Del Gratta C, Romani G, Tecchio F. Does cerebrovascular disease affect the coupling between neuronal activity and local haemodynamics. Brain. 2004; 127:99–110. [PubMed: 14570819]

Saghatelyan AK, Dityatev A, Schmidt S, Schuster T, Bartsch U, Schachner M. Excitatory transmission, and impaired extracellular matrix glycoprotein tenascin-R. Mol Cell Neurosci. 2001; 17:226–240. DOI: 10.1006/mcne.2000.0922 [PubMed: 11161481]

Salinet A, Panerai R, Robinson T. The longitudinal evolution of cerebral blood flow regulation after acute ischaemic stroke. Cerebrovasc Dis Extra. 2014; 4:186–97. [PubMed: 25298773]

Schroeter A, Grandjean J, Schlegel F, Saab BJ, Rudin M. Contributions of structural connectivity and cerebrovascular parameters to functional magnetic resonance imaging signals in mice at rest and during sensory paw stimulation. J Cereb Blood Flow Metab. 2016; :1–15. DOI: 10.1177/0271678X16666292 [PubMed: 27233628]

Siegel J, Shulman G, Corbetta M. Measuring functional connectivity in stroke: Approaches and considerations. J Cereb Blood Flow Metab. 2017; 37:2665–2678. [PubMed: 28541130]

Siegel J, Snyder A, Ramsey L, Shulman G, Corbetta M. The effects of hemodynamic lag on functional connectivity and behavior after stroke. J Cereb Blood Flow Metab. 2016; 36:2162–2176. [PubMed: 26661223]

Silasi G, Murphy TH. Stroke and the connectome: how connectivity guides therapeutic intervention. Neuron. 2014; 83:1354–1368. DOI: 10.1016/j.neuron.2014.08.052 [PubMed: 25233317]

Soleman S, Yip PK, Duricki DA, Moon LDF. Delayed treatment with chondroitinase ABC promotes sensorimotor recovery and plasticity after stroke in aged rats. Brain. 2012; 135:1210–1223. DOI: 10.1093/brain/aws027 [PubMed: 22396394]

Sullivan JE, Hedman LD. Sensory dysfunction following stroke: incidence, significance, examination, and intervention. Top Stroke Rehabil. 2008; 15:200–217. DOI: 10.1310/tsr1503-200 [PubMed: 18647725]

Suttkus A, Rohn S, Weigel S, Glöckner P, Arendt T, Morawski M. Aggrecan, link protein and tenascin-R are essential components of the perineuronal net to protect neurons against iron-induced oxidative stress. Cell Death Dis. 2014; 5:e1119.doi: 10.1038/cddis.2014.25 [PubMed: 24625978]

Swanson RA, Morton MT, Tsao-Wu G, Savalos RA, Davidson C, Sharp FR. A semiautomated method for measuring brain infarct volume. J Cereb Blood Flow Metab. 1990; 10:290–293. DOI: 10.1038/jcbfm.1990.47 [PubMed: 1689322]

Wahl AS, Omlor W, Rubio JC, Chen JL, Zheng H, Schröter A, Gullo M, Weinmann O, Kobayashi K, Helmchen F, Ommer B, Schwab ME. Asynchronous therapy restores motor control by rewiring of the rat corticospinal tract after stroke. Science. 2014; 344:1250–1255. DOI: 10.1126/science.1253050 [PubMed: 24926013]

Watson BD, Dietrich WD, Busto R, Wachtel MS, Ginsberg MD. Induction of reproducible brain infarction by photochemically initiated thrombosis. Ann Neurol. 1985; 17:497–504. DOI: 10.1002/ana.410170513 [PubMed: 4004172]

White BR, Bauer AQ, Snyder AZ, Schlaggar BL, Lee JM, Culver JP. Imaging of functional connectivity in the mouse brain. PLoS One. 2011; 6:e16322.doi: 10.1371/journal.pone.0016322 [PubMed: 21283729]

Wieloch T, Nikolich K. Mechanisms of neural plasticity following brain injury. Curr Opin Neurobiol. 2006; 16:258–264. DOI: 10.1016/j.conb.2006.05.011 [PubMed: 16713245]

Wright P, Brier L, Bauer A, Baxter G, Kraft A, Reisman M, Bice A, Snyder A, Lee J, Culver J. Functional connectivity structure of cortical calcium dynamics in anesthetized and awake mice. PLoS One. 2017; 12:e0185759. [PubMed: 29049297]

Zeiler SR, Hubbard R, Gibson EM, Zheng T, Ng K, O'Brien R, Krakauer JW. Paradoxical Motor Recovery From a First Stroke After Induction of a Second Stroke: Reopening a Postischemic Sensitive Period. Neurorehabil Neural Repair. 2016; 30:794–800. DOI: 10.1177/1545968315624783 [PubMed: 26721868]

Zhou X, Brakebusch C, Matthies H, Oohashi T, Hirsch E, Moser M, Krug M, Seidenbecher CI, Boeckers TM, Rauch UWE, Buettner R. Neurocan is dispensable for brain development. Mol Cell Biol. 2001; 21:5970–5978. DOI: 10.1128/MCB.21.17.5970 [PubMed: 11486035]

HIGHLIGHTS

- Elimination of ECM genes affects plasticity mechanisms after stroke
- Lack of ECM components does not affect infarct size
- ECM disruption facilitates contralesional resting-state functional connectivity

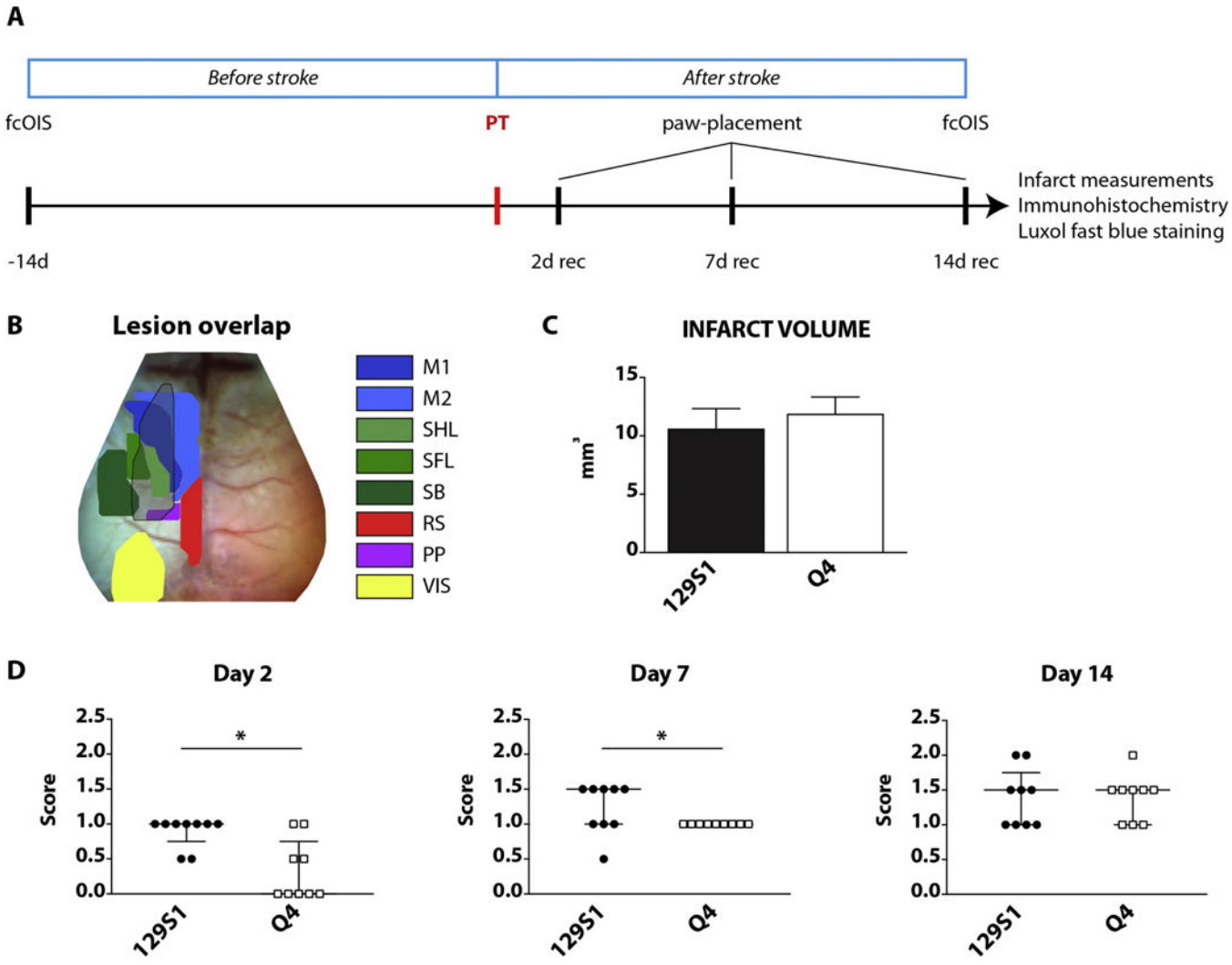

Figure 1. Experimental design, infarct volume and paw-placement test

(A) Time line of the experiments performed in this study. (B) Lesion overlay (in grey) and anatomical regions according to (Paxinos and Franklin, 2001). Primary motor (M1), secondary motor (M2), somatosensory hindlimb (SHL), somatosensory forelimb (SFL), somatosensory barrel (SB), retrosplenial (RS), posterior parietal (PP), visual (VIS). (C) Infarct volume measurements of NeuN-stained slices 14 days after stroke. Two-tailed unpaired Student's *t*-test, $n = 9$ for each group, mean ± SEM. No statistical difference was observed when comparing the two experimental groups (129S1 vs Q4 mice, $P = 0.57$). (D) Combined score for the paretic right forelimb and hindlimb in the paw-placement test at 2, 7 and 14 days of recovery. Scores are shown as individual data points with group median and interquartile range. Mann-Whitney *U*-test, $n = 9$ for each group (day 2 and day 7: $*P < 0.05$).

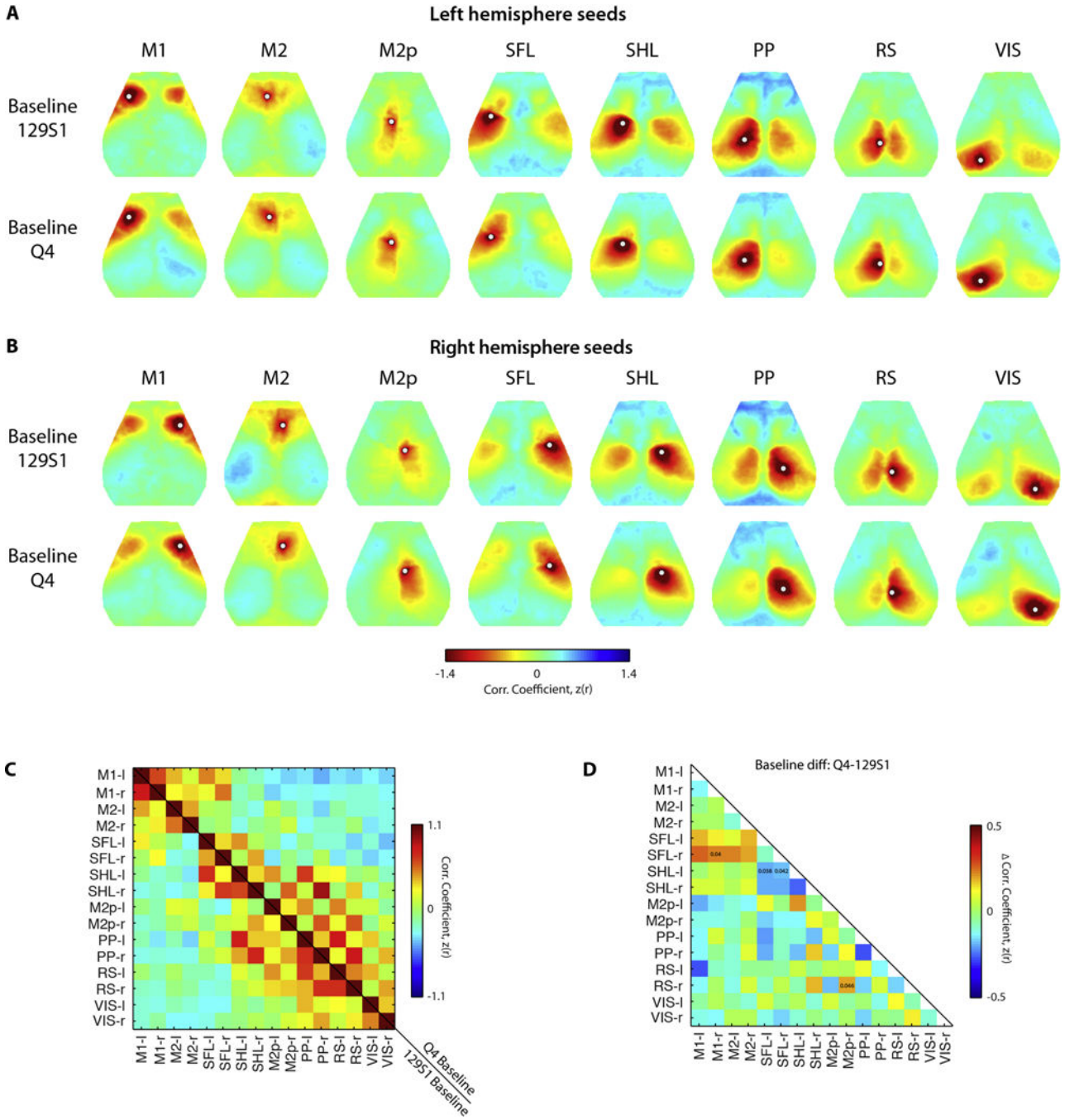

Figure 2. Maps of seed based functional connectivity patterns at baseline

Group-averaged RS-FC maps are reported between respective seed (white dot) and all other brain pixels for seeds placed in (A) left and (B) right hemisphere. The two experimental groups present similar intrahemispheric RS-FC patterns for most seed locations at baseline. However, SFL, SHL, PP, RS and VIS seeds generally exhibited less prominent interhemispheric RS-FC patterns in the Q4 group compared to the 129S1 group. (C) Seed-based interregional RS-FC matrix for Q4 (upper half) and 129S1 (lower half). (D) Group-wise RS-FC difference matrix calculated by subtracting the upper triangle from the lower

triangle (Q4 minus 129S1) of panel C does not reveal any significant differences between the groups at baseline following FDR correction, $n = 9$ for each group. M1: primary motor, M2: secondary motor, M2p: posterior secondary motor, SFL: somatosensory forelimb, SHL: somatosensory hindlimb, PP: posterior parietal, RS: retrosplenial, VIS: visual.

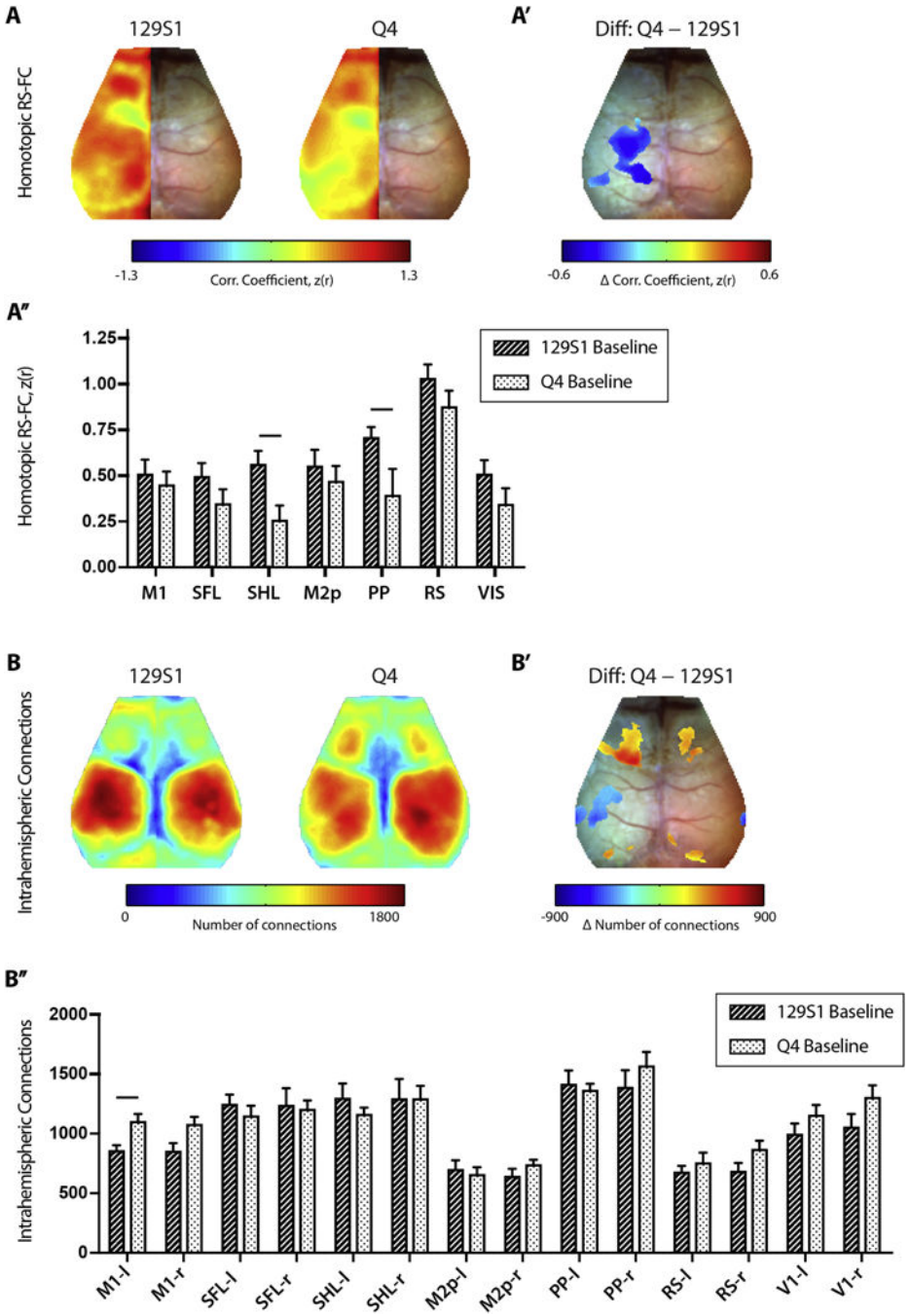

Figure 3. Baseline homotopic and intrahemispheric node degree functional connectivity maps

(A) Group-averaged homotopic correlation maps for 129S1 and Q4 mice at baseline. (A′) Difference maps indicate variations in homotopic RS-FC between Q4 and 129S1 mice (Q4 minus 129S1). (A″) Quantification of homotopic RS-FC strength in several cortical areas. Q4 mice exhibit reduced homotopic RS-FC in SHL and PP areas when compared to 129S1 mice. (B) Group-averaged intrahemispheric node degree maps for 129S1 and Q4 mice at baseline. (B′) Difference maps indicates variations in node degree between Q4 and 129S1 mice (Q4 minus 129S1). (B″) Quantification of node degree in several cortical areas. Q4

mice showed higher node degree RS-FC in M1 of the left hemisphere when compared to 129S1 mice. M1: primary motor, SFL: sensory forelimb, SHL: sensory hindlimb, M2P: posterior secondary motor, PP: posterior parietal, RS: retrosplenial, VIS: visual, l: left, r: right. Significant differences are indicated with horizontal bars (two-way ANOVA followed by FDR correction, $n = 9$ for each group, mean ± SEM, $P < 0.05$).

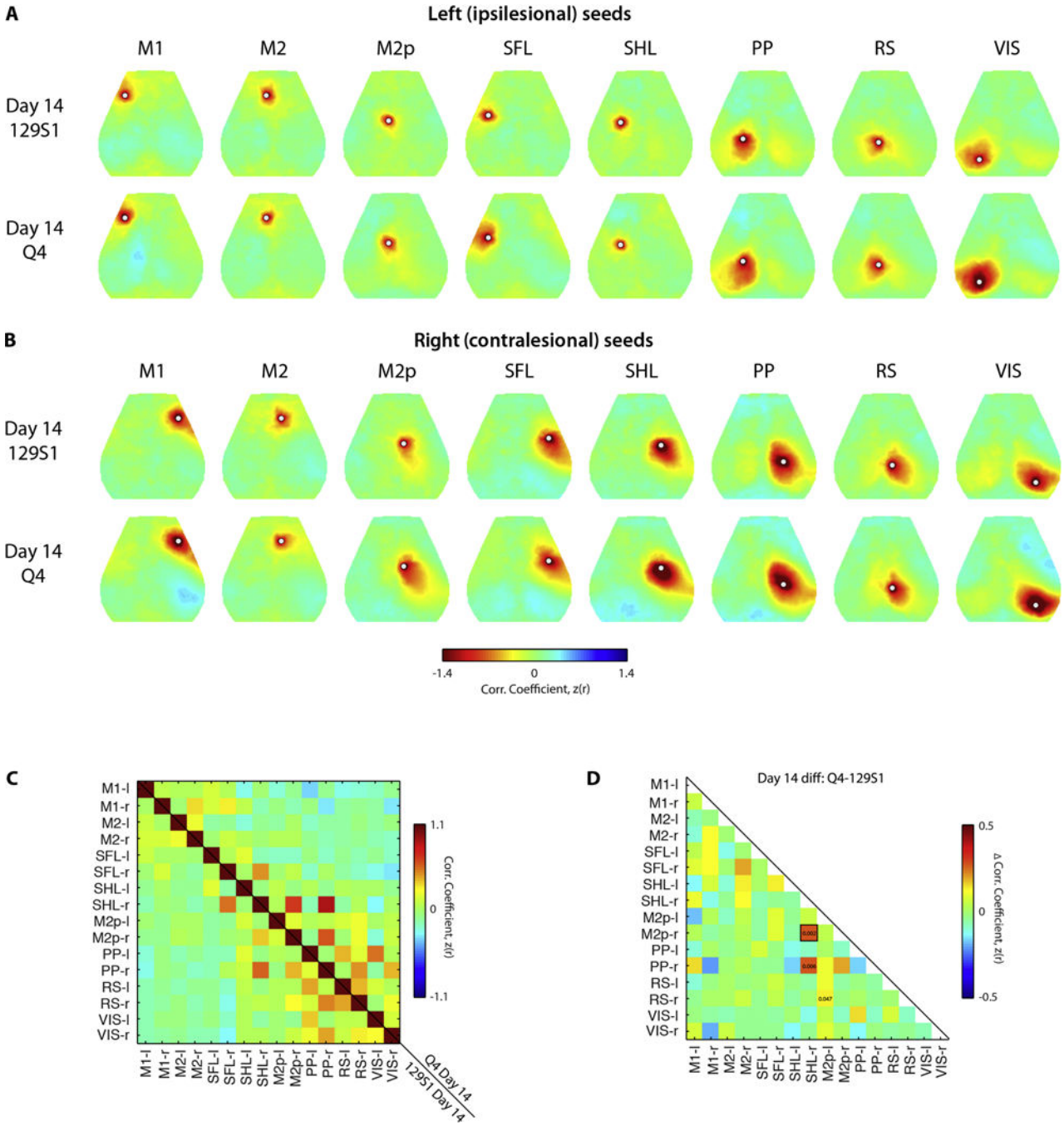

Figure 4. Maps of seed based functional connectivity patterns 14 days after stroke

Functional connectivity maps for seeds in both the (A) left (ipsilesional) and (B) right (contralesional) hemisphere present with reduced RS-FC patterns in the ipsilesional cortex and disruption of interhemispheric RS-FC in both the 129S1 and Q4 groups after stroke. Q4 mice showed more robust intrahemispheric RS-FC patterns for ipsilesional SFL, PP and VIS seeds, and contralesional M1, M2p, SHL and PP seeds compared to the 129S1 mice. (C) Seed-based interregional RS-FC matrix for Q4 (upper half) and 129S1 (lower half). (D) Group difference matrix calculated by subtracting the upper triangle from the lower triangle

(Q4 minus 129S1) evidences higher interregional RS-FC between the SHL and M2p areas of the contralesional hemisphere in Q4 mice. The black square indicates $P < 0.05$ following FDR correction, $n = 9$ for each group. M1: primary motor, M2: secondary motor, M2p: posterior secondary motor, SFL: somatosensory forelimb, SHL: somatosensory hindlimb, PP: posterior parietal, RS: retrosplenial, VIS: visual.

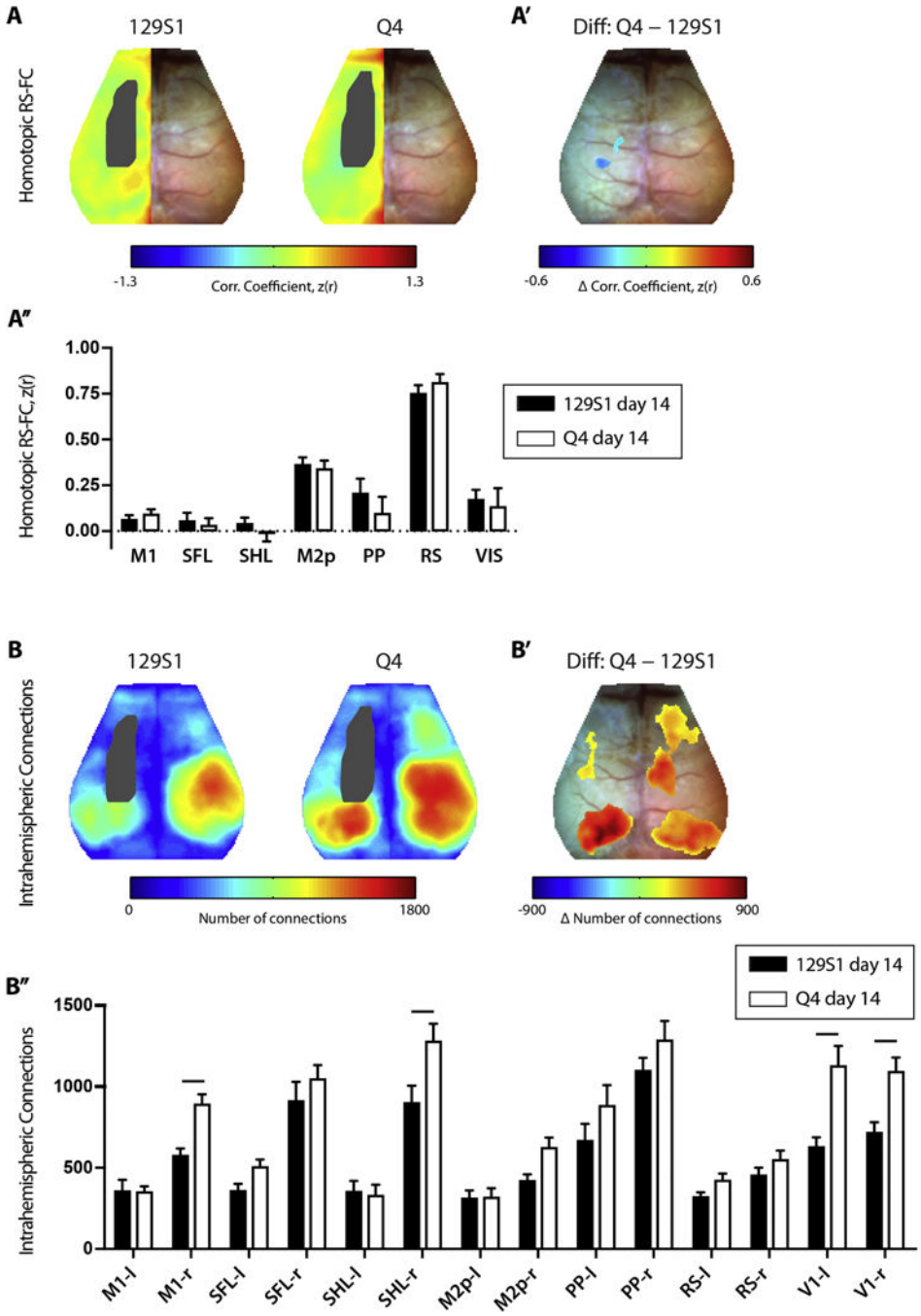

Figure 5. Post-stroke homotopic and intrahemispheric node degree functional connectivity maps

(A) Group-averaged homotopic correlation maps for 129S1 and Q4 mice at 14 days after stroke. A grey mask shows the infarct outline in the left hemisphere. (A′) Difference maps indicates variations in homotopic RS-FC between Q4 and 129S1 mice (Q4 minus 129S1). (A″) Quantification of homotopic RS-FC strength in several cortical areas indicates that after stroke the brain hemispheres become gradually less interconnected (RS-FC goes towards zero), especially in lesioned and perilesional areas of both experimental groups, such as M1, SFL, and SHL areas. Moderate homotopic connection strength remains in both

129S1 and Q4 mice in M2p, PP, RS and VIS areas. (B) Group-averaged intrahemispheric node degree maps for 129S1 and Q4 mice 14 days after stroke. (B′) Difference maps indicates variations in node degree between Q4 and 129S1 mice (Q4 minus 129S1). (B″) Quantification of node degree in several cortical areas. Q4 mice showed increased node degree RS-FC in M1 and SHL areas of the right (contralesional) hemisphere, and in both left (ipsilesional) and right (contralesional) VIS cortices when compared to 129S1 mice. M1: primary motor, SFL: sensory forelimb, SHL: sensory hindlimb, M2P: posterior secondary motor, PP: posterior parietal, RS: retrosplenial, VIS: visual, l: left, r: right. Significant differences are indicated with horizontal bars (two-way ANOVA followed by FDR correction, $n = 9$ for each group, mean ± SEM, $P < 0.05$).

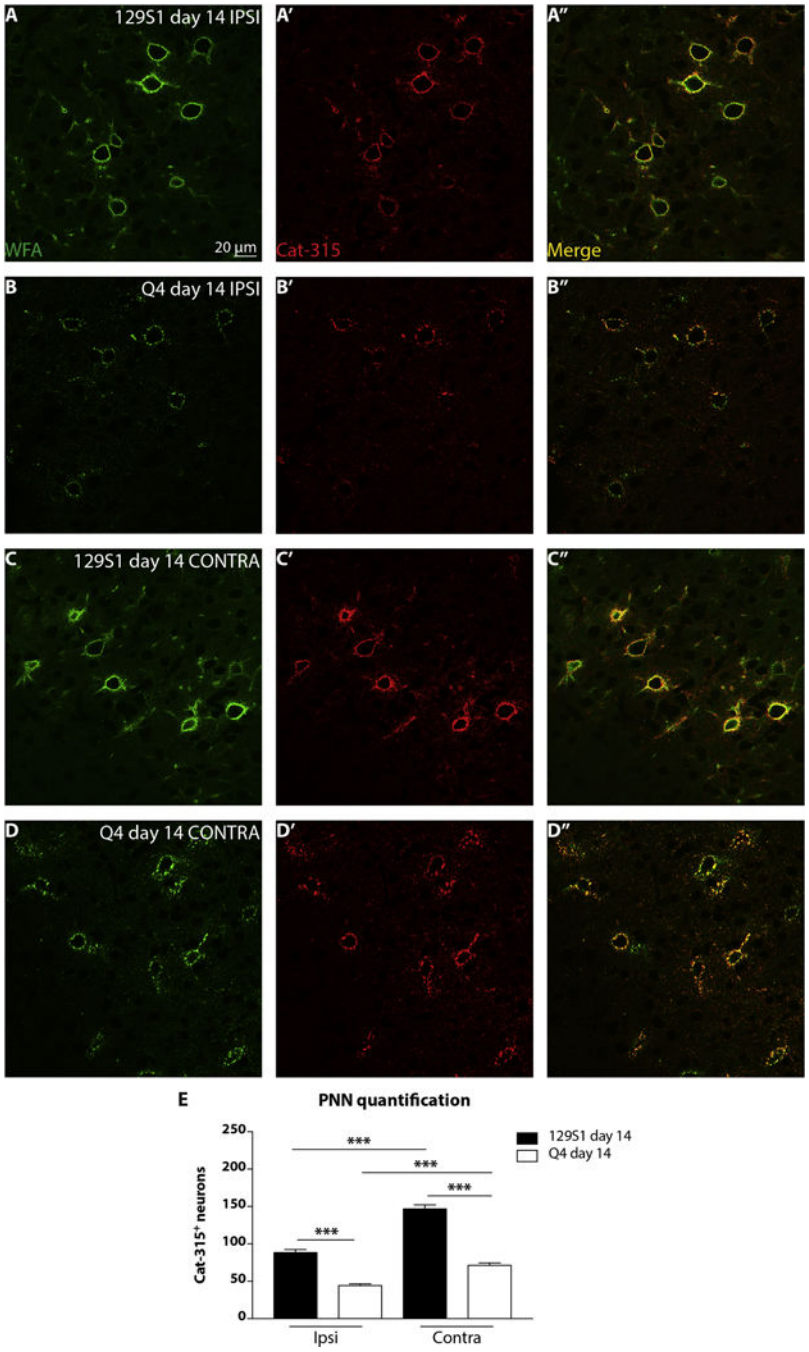

Figure 6. PNN disruption in Q4 mice after PT

Representative WFA and Cat-315 (aggrecan) double-stained brain sections 14 days after stroke. Left ipsilesional (ipsi) hemisphere in (A-A″) 129S1 and (B-B″) Q4 mice. Right contralesional (contra) hemisphere in (C-C″) 129S1 and (D-D″) Q4 mice. Note co-localization of the two markers in the majority of the cases. (E) Q4 mice show remarkable degradation of Cat-315^{+} PNNs compared to 129S1 mice, and especially in the affected hemisphere (bregma level: −0.4 mm; one-way ANOVA followed by Bonferroni correction, n = 9 for each group, mean ± SEM, ***P < 0.001).

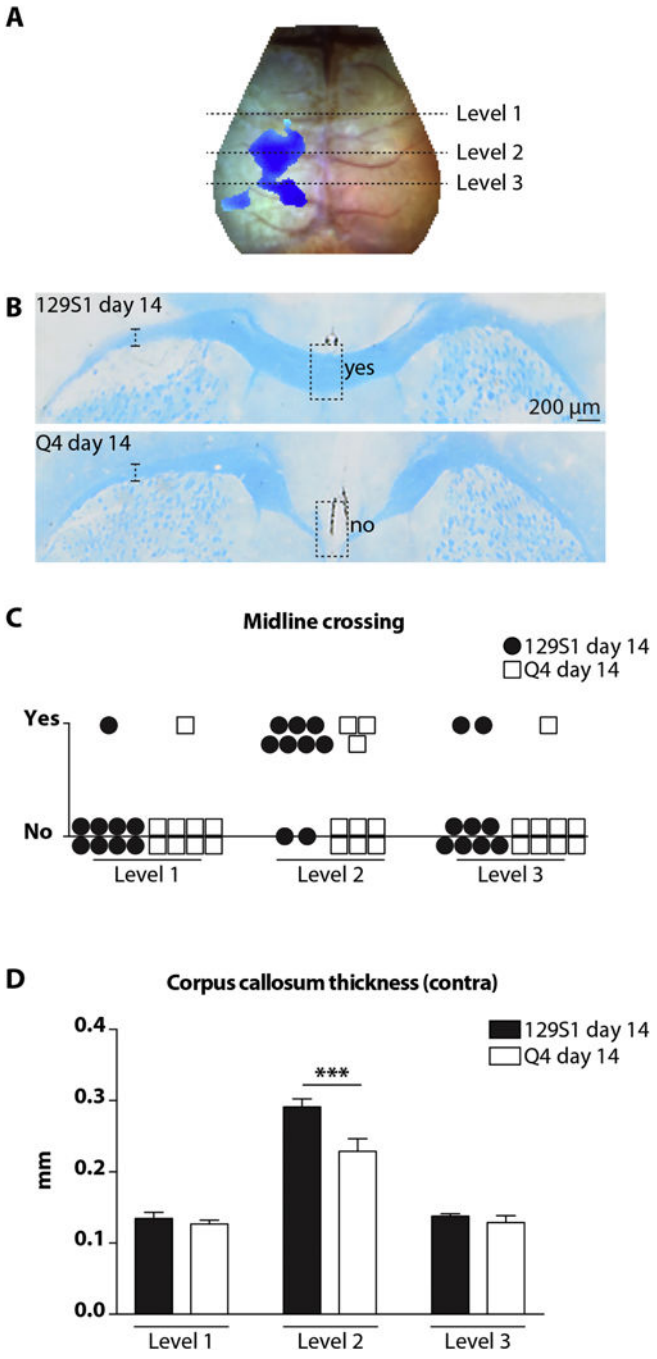

Figure 7. Changes in callosal integrity in Q4 mice after PT

(A) Callosal midline crossings were analyzed in the proximity of regions where major changes in homotopic connectivity were seen between the experimental groups (level 1: 0.98 mm; level 2: −1.06 mm; level 3: −2.06 mm from bregma). (B) Representative luxol fast blue stainings of myelin in 129S1 (first row) and Q4 mice (second row) 14 days after stroke. Note the lack of callosal midline crossing in a Q4 mice section. (C) Quantification of callosal midline crossings as in A. (D) Quantification of callosal thickness in the middle of the

unaffected (contra) hemisphere (2 mm from midline). One-way ANOVA followed by Bonferroni correction, $n = 9$ for each group, mean ± SEM (level 2: ***$P < 0.001$).

Table 1

Regional homotopic functional connectivity at baseline and 14 days after stroke

Quantification of homotopic functional connectivity in several cortical brain regions. *P* values are FDR corrected, $n = 9$ for each group, mean ± SEM. M1: primary motor, SFL: somatosensory forelimb, SHL: somatosensory hindlimb, M2p: posterior secondary motor, PP: posterior parietal, RS: retrosplenial, VIS: visual, BL: baseline, ns: not significant.

Region	(A) 129S1 BL	(B) Q4 BL	(C) 129S1 day 14	(D) Q4 day 14	P value A vs B	P value A vs C	P value B vs D	P value C vs D
M1	0.510±0.078	0.450±0.072	0.065±0.021	0.092±0.028	ns	<0.001	0.003	ns
SFL	0.500±0.073	0.350±0.078	0.057±0.043	0.032±0.038	ns	<0.001	0.001	ns
SHL	0.560±0.072	0.260±0.079	0.042±0.031	−0.014±0.043	0.004	<0.001	0.006	ns
M2p	0.550±0.083	0.470±0.083	0.360±0.037	0.340±0.043	ns	ns	ns	ns
PP	0.710±0.057	0.390±0.140	0.210±0.078	0.096±0.091	0.003	<0.001	0.003	ns
RS	1.000±0.075	0.880±0.086	0.750±0.045	0.810±0.045	ns	0.008	ns	ns
VIS	0.510±0.075	0.350±0.085	0.170±0.051	0.130±0.099	ns	0.001	0.031	ns

Table 2

Intrahemispheric node degree functional connectivity at baseline and 14 days after stroke

Quantification of node degree FC in several cortical brain regions. *P* values are FDR corrected, $n = 9$ for each group, mean ± SEM. M1: primary motor, SFL: somatosensory forelimb, SHL: somatosensory hindlimb, M2p: posterior secondary motor, PP: posterior parietal, RS: retrosplenial, VIS: visual, BL: baseline, l: left hemisphere, r: right hemisphere ns: not significant.

Region	(A) 129S1 BL	(B) Q4 BL	(C) 129S1 day 14	(D) Q4 day 14	P value A vs B	P value A vs C	P value B vs D	P value C vs D
M1-l	858±46	1102±64	358±68	353±33	ns	<0.001	<0.001	ns
M1-r	854±68	1078±64	578±41	892±61	ns	0.043	ns	0.015
SFL-l	1248±79	1151±83	360±40	508±43	ns	<0.001	<0.001	ns
SFL-r	1238±142	1205±74	914±115	1049±83	ns	0.029	ns	ns
SHL-l	1299±122	1163±57	357±62	331±65	ns	<0.001	<0.001	ns
SHL-r	1294±166	1295±105	903±103	1281±106	ns	0.002	ns	0.002
M2p-l	701±73	658±61	315±46	319±55	ns	0.004	0.004	ns
M2p-r	643±64	742±40	422±37	626±60	ns	ns	ns	ns
PP-l	1417±113	1366±52	669±102	885±124	ns	<0.001	<0.001	ns
PP-r	1389±142	1570±115	1101±77	1287±117	ns	0.032	0.032	ns
RS-l	680±50	757±83	323±26	424±40	ns	0.006	0.006	ns
RS-r	685±68	871±70	455±46	550±56	ns	ns	0.013	ns
VIS-l	996±91	1156±86	630±57	1130±121	ns	0.005	ns	<0.001
VIS-r	1056±109	1305±100	719±62	1094±85	ns	0.010	ns	0.003